Supplementary information for

Elucidating *d-d* orbital hybridization in metal-doped MnO_2 for N_2O formation inhibition mechanism in NH_3-SCR

Kai Xie[a], Ying Wang[a], Fenghui Li[a], Haiqiao Wei[a], Lei Zhou[a*]

[a] State Key Laboratory of Engines, School of Mechanical Engineering, Tianjin University, Tianjin 300072, China

The corresponding author's Email address: lei.zhou@tju.edu.cn

Calculation details

The adsorption energy E_{ad} of a species indicates its adsorption strength on the catalyst surface, and it can be described by the following Equation (1):

$$E_{ad} = E[ad/surf] - E[surf] - E[ad] \quad (1)$$

where, $E[ad/surf]$, $E[surf]$, and $E[ad]$ are the total energies of the optimized adsorbate/surface system, the clean surface, and the adsorbates in the gas phase, respectively.

Binding Energy is an important indicator for assessing the interaction strength among catalyst components, while Formation Energy signifies the feasibility of catalyst formation under specific conditions.[1, 2] E_{bind} and E_{form} are calculated using Equation (2) and Equation (3), respectively.

$$E_{bind} = E[TM/surf] - E[TM] - E[Mn\ defect/surf] \quad (2)$$

$$E_{form} = E[TM/surf] - E[surf] - \mu_{TM} + \mu_{Mn} \quad (3)$$

where, $E[TM/surf]$, $E[TM]$, $E[Mn\ defect/surf]$, and $E[surf]$ represent the total energies of the optimized transition metal-doped surface, single transition metal atom (calculated using free metal atoms), the surface with a Mn vacancy, and intact surface, respectively. μ_{TM} and μ_{Mn} are the chemical potentials of the transition metal atom and the Mn atom (calculated using bulk metal).

According to Nørskov[3], the catalytic selectivity can be assessed by the difference in the energy barriers of different reaction pathways, with a larger barrier difference corresponding to higher selectivity.

The turnover frequency (TOF) is the rate of the reactions computed per active site of the catalysts, and the Eyring-Polanyi equation from transition state theory (TST) was used to calculate the rate constant *k* and was shown in Equation (4)[2]:

$$k = \frac{\kappa k_B T}{h} exp\left(-\frac{\Delta G}{k_B T}\right) \quad (4)$$

where, k_B, h, T are the Boltzmann constant, Planck constant, and temperature, respectively. κ is the transmission coefficient assumed to be 1, meaning that all transition-state species will proceed to the product. The ΔG is the Gibbs free energy of activation, which is the Gibbs free energy difference between transition-state species and reactant species.

Table S1. Convergence tests for k-points mesh on β-MnO_2 (110) surface

k-points mesh	Energy(eV)	Energy difference(eV)
3 3 1	-543.6595006	-
2 5 1	-543.4735007	1.467
3 4 1	-543.6151334	-0.142
3 51	-543.6139412	0.001
4 4 1	-543.6139067	0.000
4 5 1	-543.6139999	0.000

All 15 irreducible single-atom doping configurations were generated by Disorder[4] software. Below are their schematic diagrams, as well as the corresponding energy values of MnO_2 doped with Ti, Fe, and Ni in these configurations.

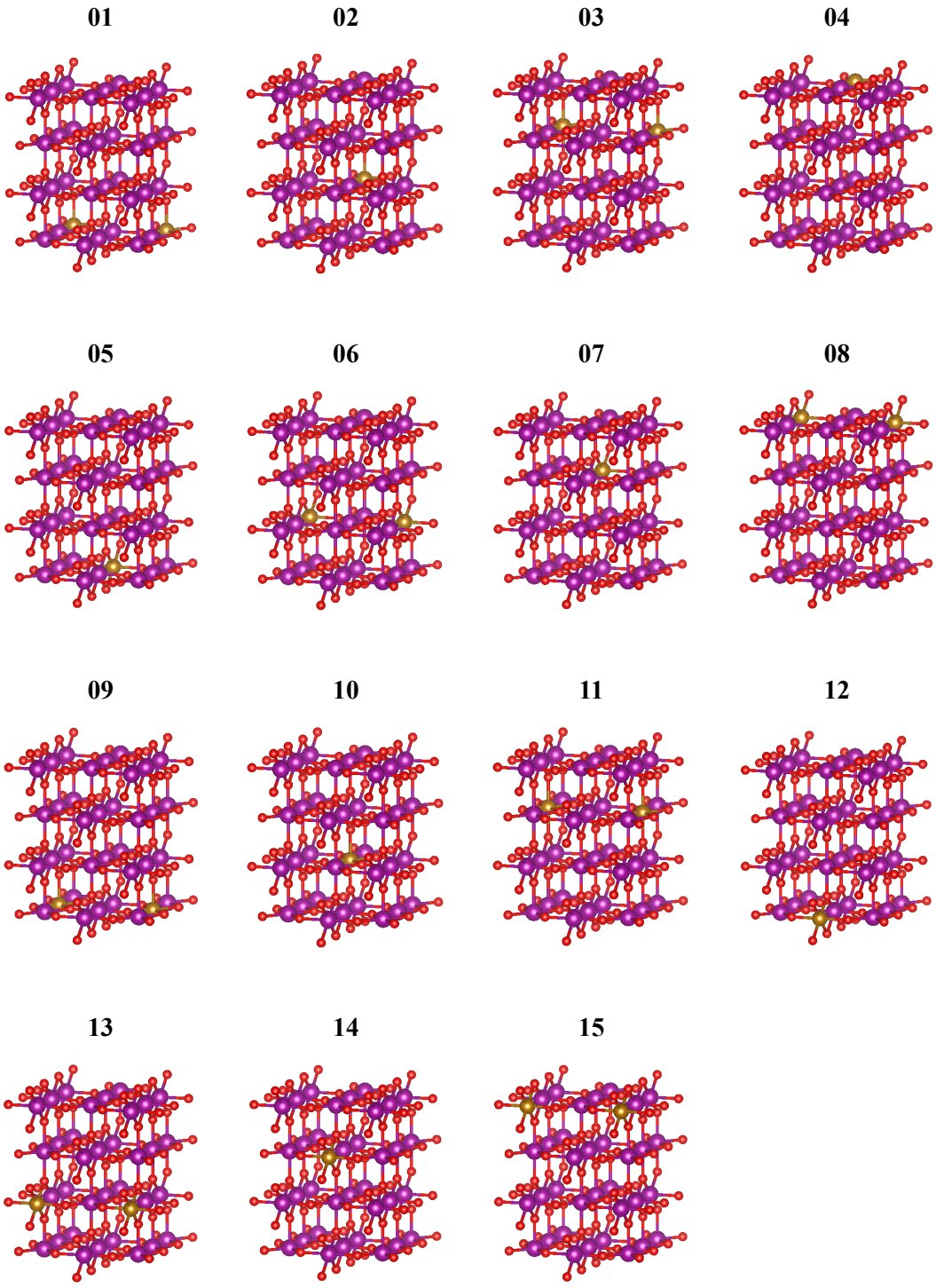

Figure S1. All possible single-atom doping configurations of MnO_2 (taking Fe-MnO_2 as an example).

Table S2. The corresponding energy of MnO_2 doped with Ti, Fe, and Ni in 15 irreducible single-atom doping configurations

No.	Ti	Fe	Ni
01	-538.2091434	-542.1995365	-537.5558400
02	-538.1499611	-541.3666071	-536.2851360
03	-538.1926099	-541.5363427	-537.6112322
04	-538.5771391	-542.222588	-538.2091434
05	-537.8742183	-541.5360085	-536.9089808
06	-537.7456637	-541.9103257	-537.9620351
07	-538.2508225	-541.8857937	-537.7311787
08	-538.3574852	-541.3867823	-536.4922522
09	-538.2642757	-541.2682171	-537.9697269
10	-537.8455683	-541.5355942	-536.7972125
11	-537.8831937	-541.6050152	-537.5011715
12	-538.2817984	-541.4695614	-537.5192964
13	-538.2813833	-541.8475724	-536.4941868
14	-538.155583	-541.887158	-537.874319
15	-538.2042995	-541.4056598	-537.4021306

Table S3. Bader charge of TM-MnO_2.

	Mn	O1	O2	TM(or Mn*)
Sc	1.735108	-0.966893	-0.966856	1.897213
Ti	1.661230	-0.969791	-0.969745	1.975523
V	1.656847	-0.920148	-0.920236	1.938791
Cr	1.670133	-0.941639	-0.941698	1.780946
Mn	1.680552	-0.932879	-0.932958	1.741108
Fe	1.713205	-0.936763	-0.936816	1.707520
Co	1.724362	-0.894240	-0.885994	1.418122
Ni	1.726992	-0.857605	-0.857584	1.322357
Cu	1.754564	-0.873837	-0.880195	1.174995

Mn* represents the Mn atom replaced by TM.

a

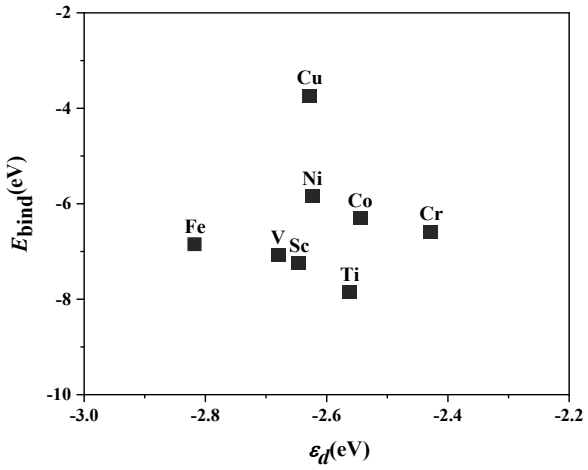

b

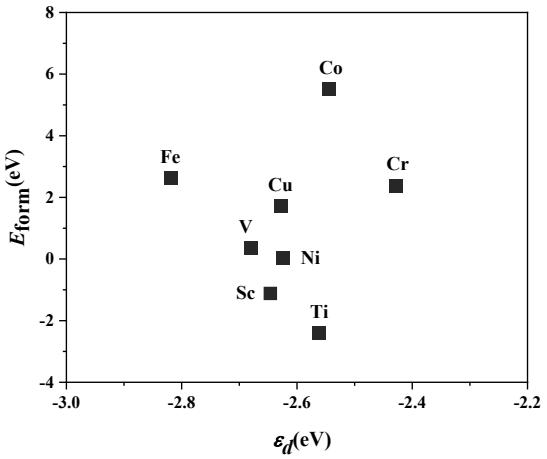

Figure S2. The relationship between the *d*-band center ε_d and (a) binding energies E_{bind} and (b) formation energies E_{form} of TM-MnO_2.

Taking NH_3 as a case study (matched its cell dimension to that of the MnO_2 catalyst), we performed projected density of states (PDOS) calculations for it, and concurrently identified the highest occupied molecular orbital (HOMO) and the lowest unoccupied molecular orbital (LUMO)[5, 6], which are depicted in **Figure S3**a and **Figure S3**b. Observations indicate that electrons on the HOMO of NH_3 surround the nitrogen (N) atom rather than being distributed along the N-H axis, suggesting that these electrons do not participate in the binding of N-H. Therefore, we speculate that the HOMO is occupied by a pair of non-bonding lone pair electrons. To support our speculation, we calculated the Electron Localization Function (ELF) of NH_3, with the results presented in **Figure S3**c. This figure clearly demonstrates the presence of non-bonding lone pair electrons surrounding N, aligning with the findings of previous studies.[7] Furthermore, the electron density on the LUMO along the N-H axis is exhibited but does not occupy the space between the N-H bond, which reveals that the LUMO of NH_3 is of an N-H antibonding orbital. By combining the atomic orbitals depicted in **Figure S3**a with the HOMO and the LUMO presented in **Figure S3**b (more MO information is provided in **Figure S4**), we can draw a preliminary conclusion: The non-bonding lone pair electrons on the HOMO of NH_3 originate from the sp^3 hybridization involving the $2p_z$ orbital of N, and these electrons are crucial to its reactivity. Meanwhile, the sp^3 hybridized $2p_x$ and $2p_y$ orbitals form bonds with the 1*s* orbitals of H. Based on these findings, we can illustrate a schematic diagram of the molecular orbitals of NH_3 in **Figure S3**d.

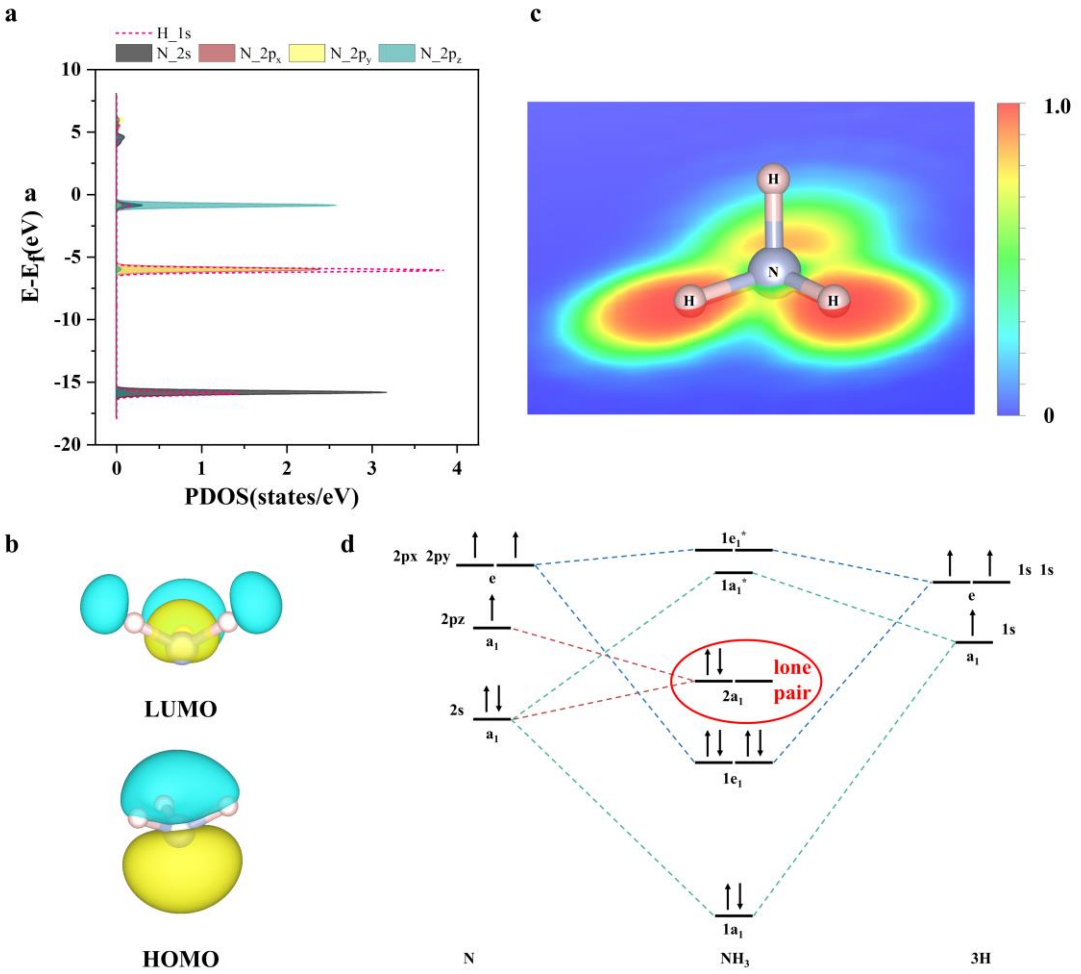

Figure S3 (a)-(d) Projected density of states, highest occupied molecular orbital and lowest unoccupied molecular orbital, electron localization function, and molecular orbitals schematic diagram of NH_3.

a

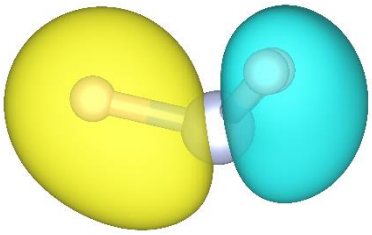

HOMO-1

b

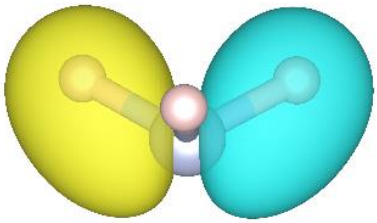

c

HOMO-2

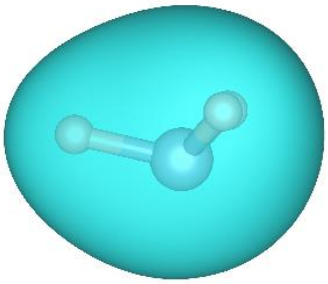

HOMO-3

Figure S4. More molecular orbitals under the highest occupied molecular orbital of NH_3.

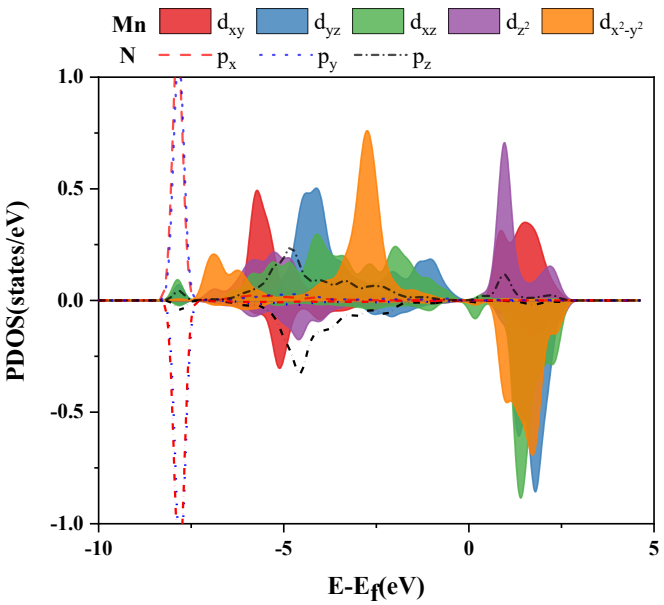

Figure S5. The density of states of pristine MnO_2 adsorbing NH_3 includes spin-up and spin-down.

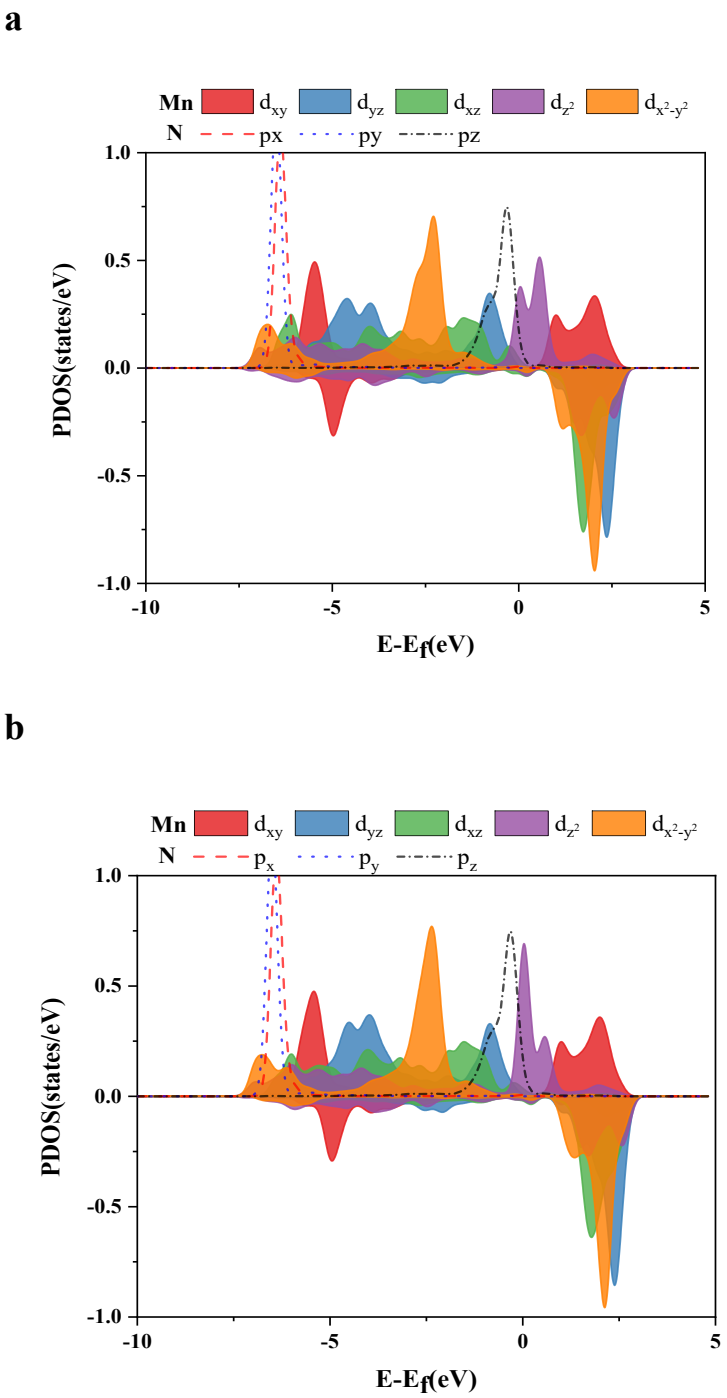

Figure S6. Projected density of states of (a)-(b) Mn site1 and Mn site2 at the opposite ends in bridge-site adsorption.

a

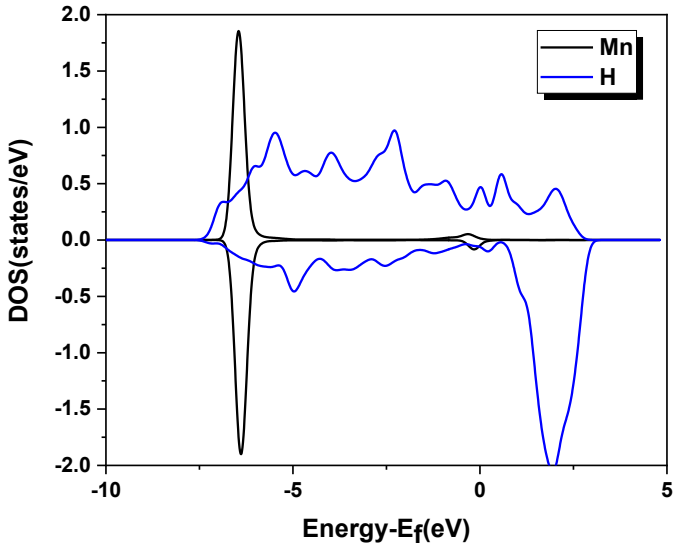

b

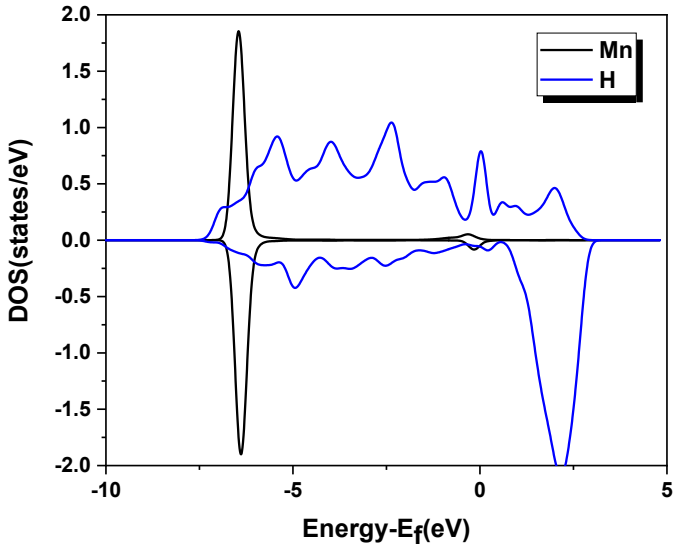

Figure S7. Projected density of states of (a) Mn site1 and (b) Mn site2 at the opposite ends in bridge-site adsorption and the H of NH_3.

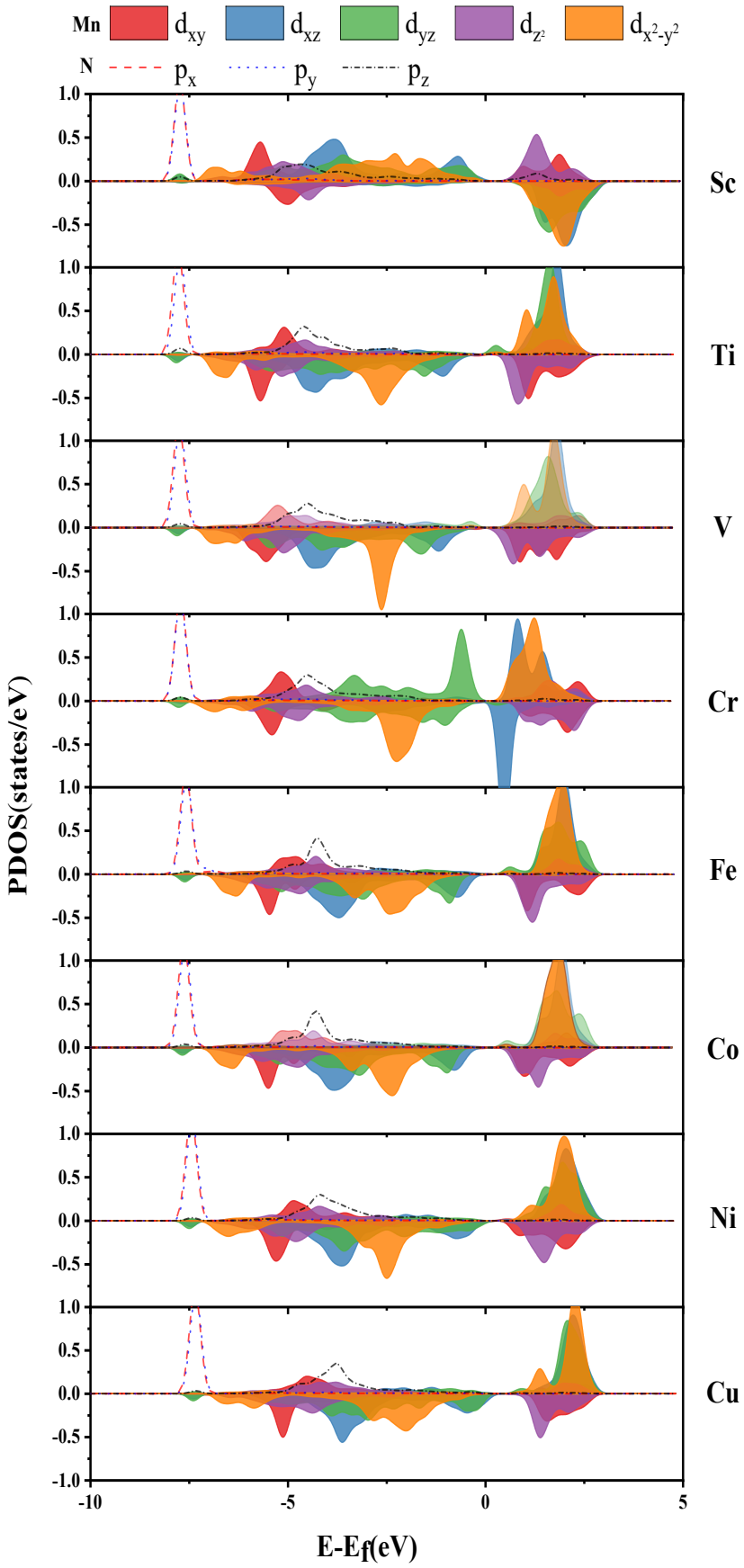

Figure S8. Projected density of states of TM-MnO_2 in top-site adsorption.

For the TM-MnO_2 system, the adsorption site of NH_3 could be either the Mn site or the TM site. Computational results indicate that all TM-MnO_2 catalysts still favor the Mn site as the most stable adsorption site.

Table S4. The adsorption energies of NH_3 on the Mn site and TM site of TM-MnO_2

TM-MnO_2	Adsorption energy at Mn site (eV)	Adsorption energy at Tm site (eV)
Sc-MnO_2	-1.15	-0.97
Ti-MnO_2	-1.74	-1.25
V-MnO_2	-1.23	-1.11
Cr-MnO_2	-1.32	-1.07
Fe-MnO_2	-2.23	-1.86
Co-MnO_2	-0.81	-0.68
Ni-MnO_2	-2.07	-1.79
Cu-MnO_2	-0.76	-0.57

For the TM-MnO_2 system, computational results indicate that the energy barriers of the rate-determining steps for both N_2 and N_2O formation are higher than those on the Mn sites in all TM-MnO_2 catalysts.

Table S5. The energy barriers of the rate-determining steps for both N_2 and N_2O formation on the TM site (TS2 and TS4)

Energy barriers	Fe-MnO_2		Ti-MnO_2		Ni-MnO_2	
	Mn	**Fe**	**Mn**	**Ti**	**Mn**	**Ni**
TS2	1.23	1.52	0.84	1.21	1.15	1.4
TS4	0.38	1.19	0.44	1.11	0.48	1.27

a

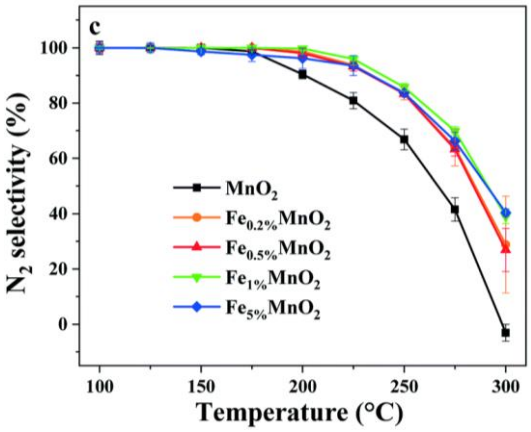

b

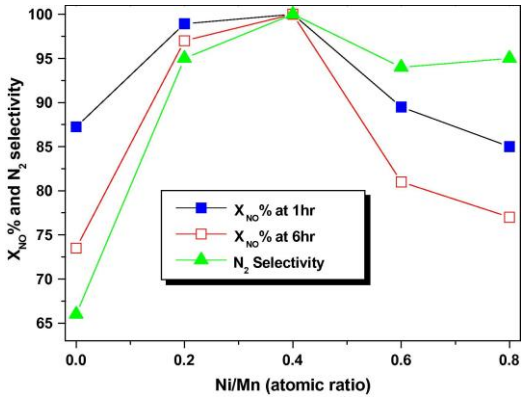

c

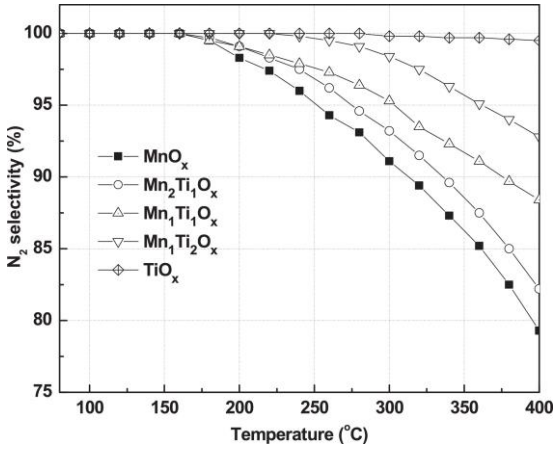

Figure S9. The relevant experimental data from the literature support that (a) Fe-MnO_2[8], (b) Ni-MnO_2[9], and Ti-MnO_2[10] catalysts can effectively inhibit N_2O formation.

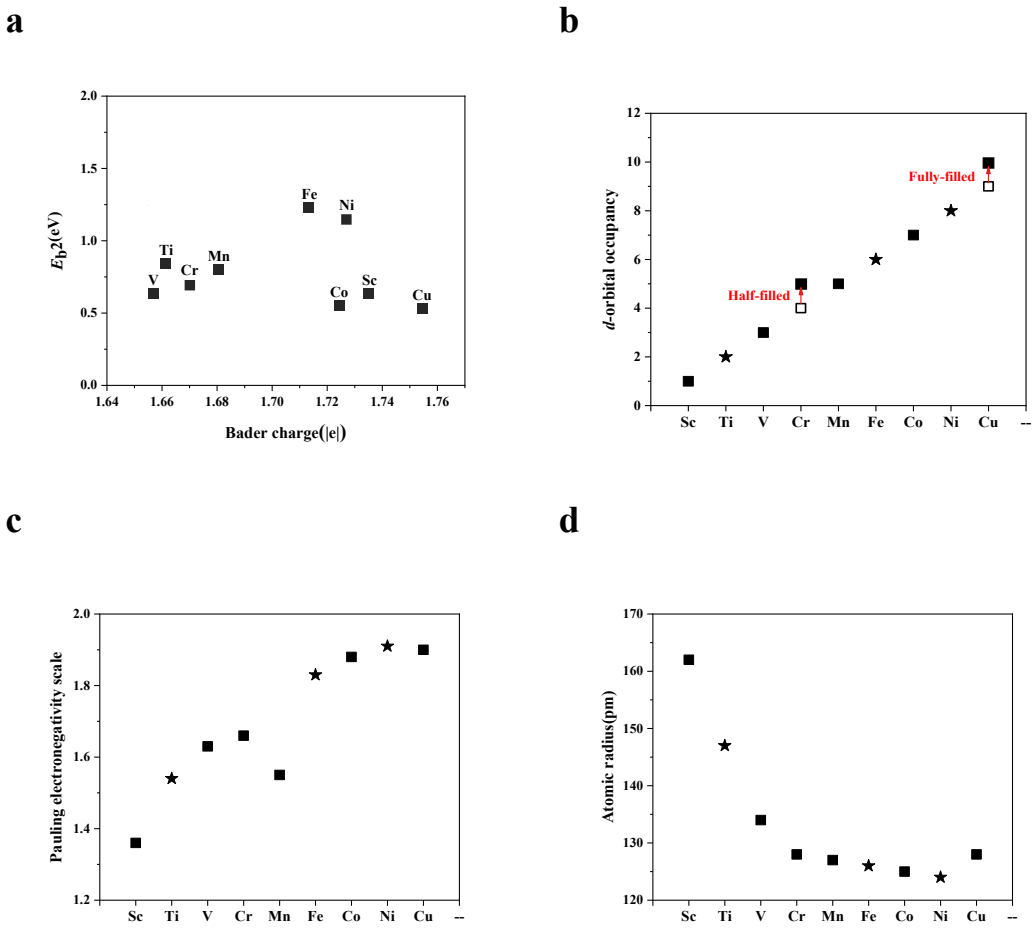

Figure S10. (a) Bader charge values of Mn site of TM-MnO_2, (b) *d*-orbital occupancy, (c) Pauling electronegativity scale, and (d) atomic radius of the dopant in TM-MnO_2.

Table S6. The t_{2g}-e_g configuration of the TM ion in TM-doped MnO_2

Transition metal	Main oxidation state	t_{2g}-e_g configuration
Sc	Sc^{3+}	$t_{2g}^0 e_g^0$
Ti	Ti^{4+}	$t_{2g}^0 e_g^0$
V	V^{4+}	$t_{2g}^1 e_g^0$
Cr	Cr^{3+}	$t_{2g}^3 e_g^0$
Fe	Fe^{3+}	$t_{2g}^3 e_g^2$
Co	Co^{3+}	$t_{2g}^6 e_g^0$
Ni	Ni^{2+}	$t_{2g}^6 e_g^2$
Cu	Cu^{2+}	$t_{2g}^6 e_g^3$

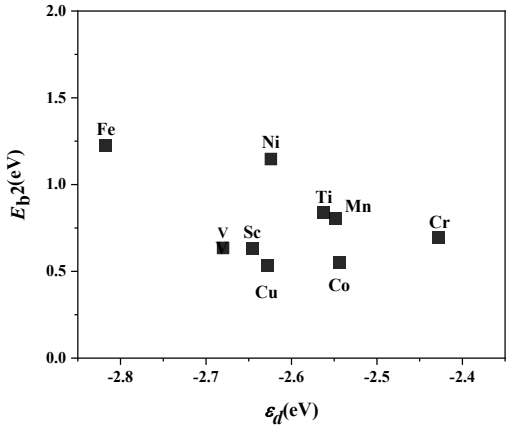

Figure S11. *d* orbital center of Mn site of TM-MnO_2.

a

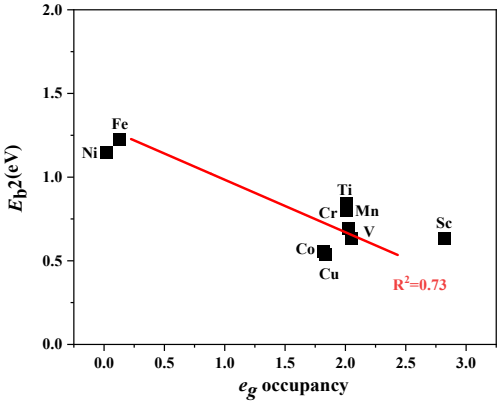

b

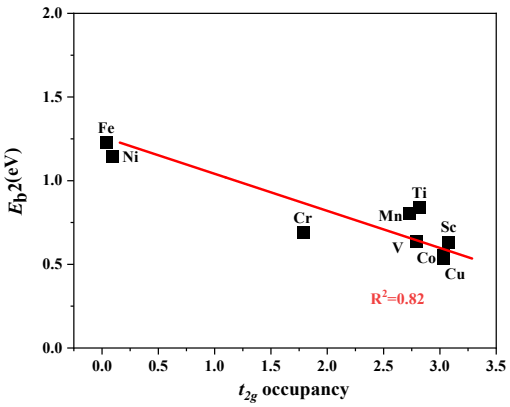

Figure S12. (a) the e_g occupancy; (b) t_{2g} occupancy of the Mn active site in transition metal-doped MnO_2.

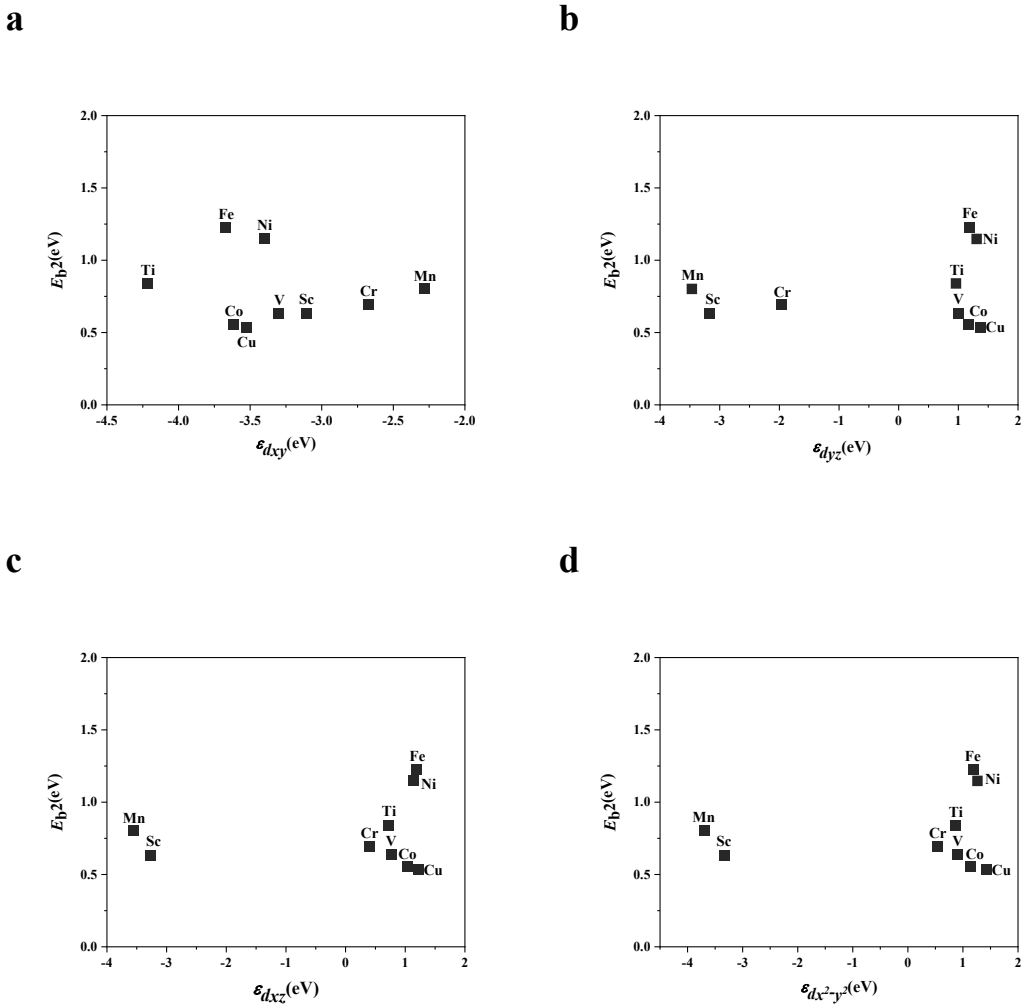

Figure S13. The correlation between the highest energy barrier of N_2O formation E_{b2} and (a) the d_{xy} orbital center $\varepsilon_{d_{xy}}$; (b) the d_{yz} orbital center $\varepsilon_{d_{yz}}$; (c) the d_{xz} orbital center $\varepsilon_{d_{xz}}$; (d) the $d_{x^2-y^2}$ orbital center $\varepsilon_{d_{x^2-y^2}}$.

a

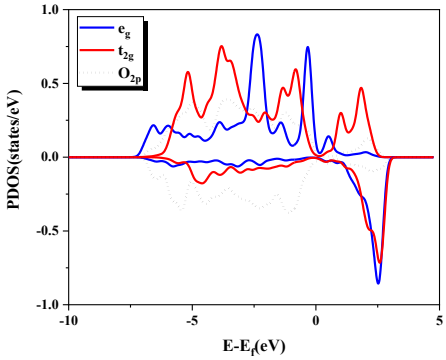

b

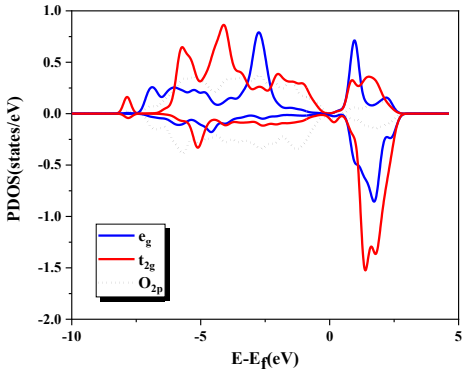

c

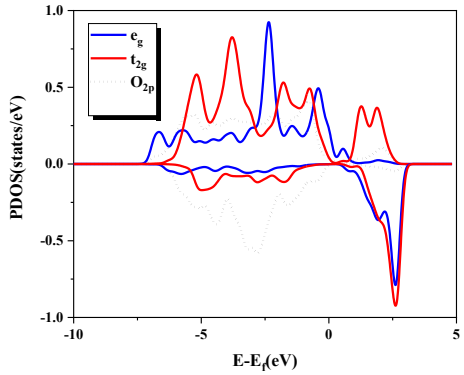

Figure S14. The PDOS of (a) MnO_2, (b) NH_3 adsorbed on MnO_2, and (c) Ti-doped MnO_2, specifically focusing on the e_g, t_{2g}, and O_{2p} orbitals.

a

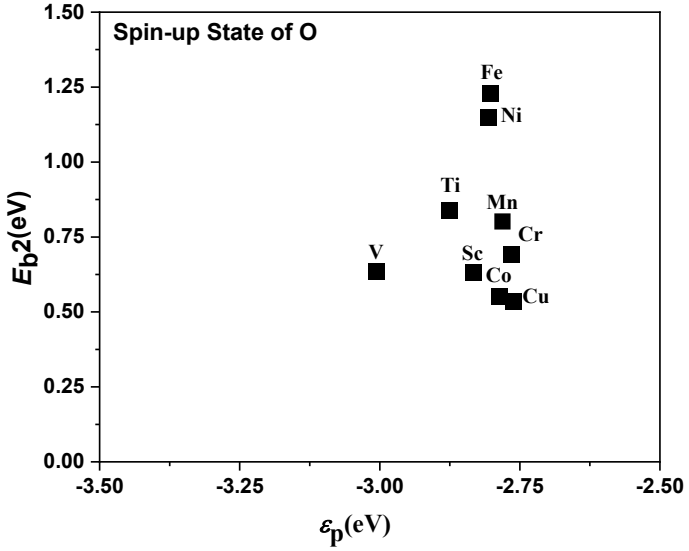

b

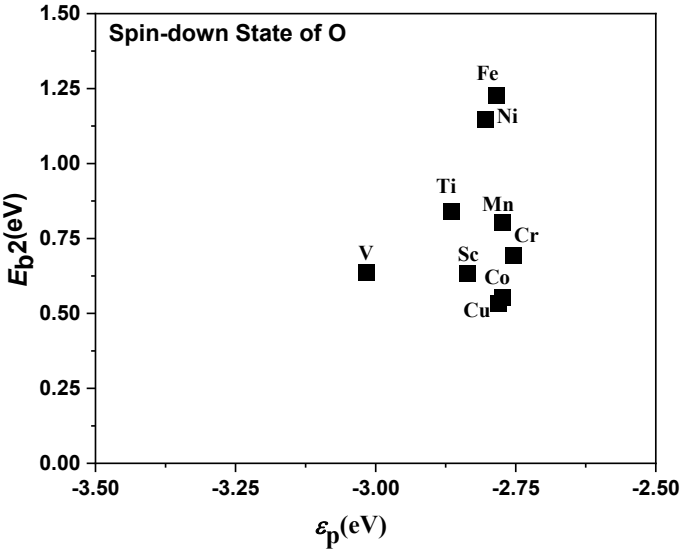

Figure S15. The correlation between the highest energy barrier of N_2O formation E_{b2} and the *p* band center ε_p of O in (a) spin-up state and (b) spin-down state.

References

1. K. Yang, Y. Dai and B. Huang, *Chem. Phys. Lett.*, 2008, **456**, 71-75.
2. C. He, C. H. Lee, L. Meng, H. T. Chen and Z. Li, *J. Am. Chem. Soc.*, 2024, **146**, 12395-12400.
3. J. K. Nørskov, T. Bligaard, J. Rossmeisl and C. H. Christensen, *Nat. Chem.*, 2009, **1**, 37-46.
4. J.-C. Lian, H.-Y. Wu, W.-Q. Huang, W. Hu and G.-F. Huang, *Physical Review B*, 2020, **102**, 134209.
5. V. Wang, N. Xu, J. C. Liu, G. Tang and W. T. Geng, *Comput. Phys. Commun.*, 2021, **267**, 108033.
6. K. Momma and F. Izumi, *J. Appl. Crystallogr.*, 2008, **41**, 653-658.
7. N. V. Cohan and C. Coulson, *Trans. Faraday Soc.*, 1956, **52**, 1163-1172.
8. H. Fan, J. Fan, T. Chang, X. Wang, X. Wang, Y. Huang, Y. Zhang and Z. Shen, *Catal. Sci. Technol.*, 2021, **11**, 6553-6563.
9. B. Thirupathi and P. G. Smirniotis, *J. Catal.*, 2012, **288**, 74-83.
10. S. Shu, J. Guo, J. Li, N. Fang and S. Yuan, *J. Taiwan Inst. Chem. Eng.*, 2019, **100**, 168-177.